IEEE Open Journal of Vehicular Technology

Received XX Month, XXXX; revised XX Month, XXXX; accepted XX Month, XXXX; Date of publication XX Month, XXXX; date of current version January 16, 2025.

Digital Object Identifier 10.1109/OJVT.2024.0627000

Comparative Analysis of a Low-voltage CHB Inverter without PWM and Two-Level IGBT/SiC Inverters for Electric Vehicles on Driving Cycles

GAËL PONGNOT[1], ANATOLE DESREVEAUX[1,2] (Member, IEEE), CLÉMENT MAYET[3] (Member, IEEE), DENIS LABROUSSE[1,2], AND FRANCIS ROY[4]

[1]Université Paris-Saclay, ENS Paris-Saclay, CNRS, SATIE, F-91190, Gif-sur-Yvette, France
[2]Le Conservatoire national des arts et métiers (Cnam), Paris, F-75003, France, HESAM Université
[3]Univ. Lille, Arts et Métiers Institute of Technology, Centrale Lille, Junia, ULR 2697 – L2EP, Lille, F-59000, France
[4]Stellantis, Technology Office, F-78955 Carrières-sous-Poissy, France

CORRESPONDING AUTHOR: Gaël Pongnot (e-mail: gael.pongnot@ens-paris-saclay.fr).

This work was supported by a grant overseen by the French Agency for Ecological Transition (ADEME).

ABSTRACT Electric Vehicles (EVs) based on Cascaded H Bridge (CHB) promise reduced consumption and improved modularity, repairability, resilience, and versatility. This study focuses on evaluating the efficiency of CHB inverters utilizing low-voltage Si MOSFETs to improve EV performance and range. Through a comprehensive system-level approach and modeling, a simulation of the CHB-based powertrain is developed and experimentally validated. Electrical and mechanical simulations are conducted separately and finally combined to streamline computation times. Subsequently, CHB-based EV is compared with standard two-level inverters (2LI) across different driving cycles, considering multiple sources of losses from the battery to the road. Despite increased battery losses, CHB proves reduction of consumption during urban driving cycles, making it a compelling choice for sustainable commuter vehicles.

INDEX TERMS Cascaded H-bridge (CHB), Modular multilevel converter (MMC), Multilevel inverter (MLI), Multilevel battery storage system (BSS), SiC inverter, Energetic macroscopic representation (EMR), Driving cycle, Loss evaluation, Electric Vehicles

I. INTRODUCTION

Limiting global warming to 1.5 °C demands rapid and deep cuts in greenhouse gas emissions [1]. Introducing carbon budgets and striving for net zero emissions are vital steps. Road transportation contributes one-sixth of global greenhouse gases (GHG) emissions [2].

Electric vehicles powered by low-GHG electricity, coupled with improved vehicle usage, could be transformative in this regard [1], [2]. In 2022, EVs accounted for 21% of European sales [3]. To penetrate the market further, EVs need better range and cost, achievable through higher battery energy density and improved drivetrain efficiency. Battery durability depends on vehicle usage [4], [5]. Addressing these issues requires improving energy and material efficiency in production and usage, enhancing system durability and resilience, and promoting circular material flows [1], [6].

Electric vehicles typically utilize two-level inverters (2LI), predominantly with IGBT transistors or more recently incorporating SiC MOSFETs. The performance of this vehicle architecture is well-documented [7], [8]. However, advancements can be achieved by integrating greater intelligence into batteries to improve their life duration [9], [10]. Various modular multilevel converter (MMC) structures, including the classical 6-legged MMC and Cascaded H-bridges (CHB) can be proposed for this purpose. However, achieving the same motor voltage with an MMC requires double the number of modules compared to a CHB, leading to complex control strategies and requiring additional inductors [11]. Consequently, this article focus on CHB multilevel converters, pioneered by Tolbert *et al.* [12]. The association of CHB converters with energy storage devices has recently gained in importance [9], [13], [14]. Automotive and battery storage

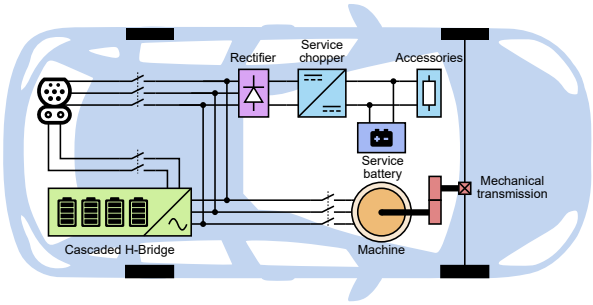

FIGURE 1. Cascaded H-Bridge inverter integrated to an electric vehicle

companies consider this architecture as a future trend, like Stellantis, Saft and others [15], [16]. This merging of energy storage with power electronics enables direct AC supply to the traction machine and eliminates the need for an onboard charger, Figs. 1 and 2. This configuration is also investigated for grid battery energy storage systems (BESS) and holds promise for V2G applications [17]–[20].

The literature typically discusses CHB configurations with 3 to 6 modules per phase [13], [14], [18], [21]–[23], requiring medium-voltage Si MOSFETs, from 80 V to 120 V for 2 or 3 modules [13], [23]. A low number of modules induce the use of high-frequency modulations to power the electric motor. Mainly papers in the literature use phase-shifted pulse-width modulation (PS-PWM) or level-shifted PWM (LS-PWM) [18], [21], [22], [24]. Using PWM increase the switching losses in the inverter.

Unlike PS-PWM, selective harmonic elimination (SHE) [12], [25], and nearest level control (NLC) [14], [26] can significantly reduce the switching frequency, but necessitating a large number of modules (greater than 10), to maintain the waveform quality. This work aims to study a CHB with 24 modules per phase, connected directly at the battery side (Fig. 1), based on a prototype developed by Stellantis [15]. This highly modular configuration decreases the battery module voltages, enhancing the safety, efficiency, and scalability of the powertrain. Thus, H-Bridges are constructed using low-voltage MOSFETs. In this study, NLC is chosen for its ease of implementation and significant reduction in switching losses.

However, NLC is rarely considered for power electronics losses evaluation due to the inability to create an average model for switching losses. So, there is a lack of knowledge and methods to evaluate the potential of such a system for EVs, as this paper wants to contribute.

Comparing performances of different structures necessitates a systemic approach with equitable modeling of each element. Battery, power electronics, and machine control strategies must be collectively examined to comprehend their mutual interactions. [25] focus on battery behavior using SHE. While [13] adopt a backward approach to compare 2LI and CHB during driving cycles, without considering battery losses. Similarly, [23] focus solely on power electronics. However, these works fail to consider the entirety of the powertrain, resulting in limited scopes and inevitable errors in efficiency evaluation, as they systematically neglect the interaction between batteries and electronics. Present study addresses this gap by comprehensively considering the various losses incurred throughout the entire powertrain, enabling a more equitable comparison with existing technologies.

The objective of this paper is to evaluate the performance of a low voltage CHB inverter for an EV application. To that aims, the paper proposes a methodology to compute the system from the high amount of battery modules (24 per phase) to the vehicle chassis. This methodology should find a compromise between highly detailed components models and reduced simulation duration.

Evaluation criteria for structures should include efficiency and consumption during constant speed sequences or realistic driving cycles [27]. Modeling and simulation results for specific operating points do not provide a fair basis for comparing a CHB inverter with existing structures, such as the 2LI. However, driving cycle simulations can spend several hours and require substantial computing capacities, particularly when considering electrical dynamics. Additionally, unlike PWM, NLC cannot be averaged to reduce computation time [13], [28]. Hence, our methodology distinguishes between electrical and mechanical dynamics to address these challenges. Therefore, a contribution is to compare CHB, IGBT and SiC inverters demonstrating the need for a systemic approach.

A novel system-level model has been developed, incorporating the entire system's losses. Unlike conventional methods that often study components individually [23], [25] or combined using a backward approach [13], our model uses a forward approach, capturing the reciprocal interactions between all subsystems.

The key contributions of this paper are as follows:

1) A CHB inverter with a high number of modules per phase (24) is proposed to power an electric vehicle (EV).
2) A methodology is developed to compute the inverter losses when using Nearest Level Control (NLC), which is integrated into a powertrain simulation.
3) The performances and losses at the component level, including the batteries and CHB inverter, are analyzed across a wide operating range.
4) The proposed vehicle's performance is evaluated and compared with current 400 V and 800 V vehicle topologies.

The following sections are organized as follows. Firstly, section II presents CHB inverter structure and its model. Our developed simulation tools are validated by comparison with real tests on CHB prototype in section III. Then, section IV shows a comparison with conventional 2LI structures, IGBT and SiC, from the model to the efficiency in the torque-speed field. Finally, section V focus on the usage of these structures for an electric vehicle, combining them with a vehicle model including mechanical simulations. Evaluation and conclusion are made on consumption during driving cycles.

This article has been accepted for publication in IEEE Open Journal of Vehicular Technology. This is the author's version which has not been fully edited and content may change prior to final publication. Citation information: DOI 10.1109/OJVT.2025.3531652 IEEE Open Journal of Vehicular Technology

II. CASCADED H-BRIDGE INVERTER MODELING

A Cascaded H-bridge inverter supplies a PMSM, Fig. 2. Three legs, each consisting of M serial modules (24 in this case), produce the phase voltages v_p. A module comprises the association of an N-cell battery (4 in this instance) with an H-bridge. As the battery cell voltage is around 4 volts, a module voltage is approximately 16 V, which allows the use of low-voltage MOSFETs for the H-bridges. To avoid the need for an on-board charger and achieve European electric grid compatibility (230-400 V), the embedded battery cells must be increased, totaling 288 cells. Eliminating the charger and placing the battery closer to the converter optimizes the available space, allowing for increased battery capacity.

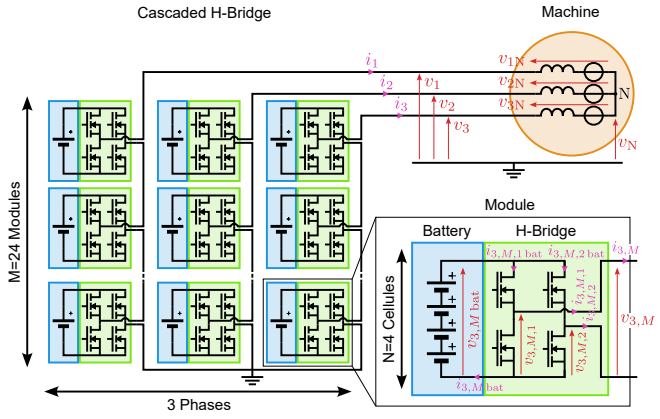

FIGURE 2. Cascaded H-Bridge inverter connected to a PMSM

A. ENERGETIC MACROSCOPIC REPRESENTATION

To address the problem posed in this article, a comprehensive system model must be developed, spanning from the battery to the wheel, and leveraging existing models available in the literature. This paper adopts the EMR formalism to organize and interconnect models based on physical energy properties. EMR formalism is commonly employed in the transport field to model and control complex and multi-source energetic systems [5], [28], [29]. EMR, derived from Bond Graph theory, provides a graphical depiction of complex systems, illustrating interactions between elements through action-reaction links while maintaining physical causality [30]. This technique effectively highlights the energetic properties of the system, enabling the deduction of control structures and strategies through model inversion [26].

The EMR of a CHB inverter connected to a machine is depicted in Fig. 3, providing the foundation for the ensuing model equations. Vector representation is employed for a concise and adaptable model, with dimensions indicated between arrows. A complete description of the model is given in [26]. The upper part of Fig. 3, in orange and green, represents the model following the equations developed from Section II.B to II.E. The lower parts, in light blue and dark blue, represent the local control scheme and the global control strategy with explanations provided in Section II.F.

B. STRUCTURE AND OPERATING MODE

The phase voltages v_p can be expressed as the sum of module voltages $v_{p,m}$, (1). Each module carry the same phase current, (2). By construction, (3) and (4) demonstrate couplings inside a module from the machine side, while (5) and (6) show the same from the battery side. Equations (1) to (6) which model the H-Bridges and there serial connections, are represented in EMR using three coupling elements : double orange squares in Fig. 3.

$$v_p = \sum_{m=1}^{M} v_{p,m} \tag{1}$$

$$i_{p,m} = i_p \tag{2}$$

$$v_{p,m} = v_{p,m,1} - v_{p,m,2} \tag{3}$$

$$i_{p,m,1} = -i_{p,m,2} = i_{p,m} \tag{4}$$

$$v_{p,m,b\,\mathrm{bat}} = v_{p,m\,\mathrm{bat}} \tag{5}$$

$$i_{p,m\,\mathrm{bat}} = i_{p,m,1\,\mathrm{bat}} + i_{p,m,2\,\mathrm{bat}} \tag{6}$$

The Nearest Level Command (NLC) is employed, leveraging the multitude of available levels. This strategy selects the nearest available level from the reference, chosen for its simplicity and reduced switching count compared to other waveform modulations. On average, each transistor switch less than twice during an electric period, making this choice pertinent given the large number of modules considered.

C. LITHIUM BATTERY CELLS

Lithium batteries are typically modeled using a serial RC network and a static resistor, which provide a reasonable approximation of cell behavior. This study adopts a static model to reduce computation time and assumes perfectly balanced battery cells with identical open-circuit voltage (OCV). The CHB inverter allows for perfect SoC balancing between cells due to its numerous modules. Several strategies have been proposed in the literature [14], [26]. The strategy described in [26] is implanted in the prototype used to validate the models (section III-B).

D. LOW-VOLTAGE SILICON MOSFETS

The H-bridge legs are controlled by a switching command $f_{p,m,b}$ for switching cells (SC), illustrated in Fig. 3, with b representing the bridge index (1 or 2). These ½-bridge experience both conduction and switching losses. Conduction losses are modeled using a voltage drop attributed to a series resistance $R_{\mathrm{DS_{on}}}$ (7). Additionally, switching losses are modeled by an additional input current $i_{p,m,b\,\mathrm{sw}}$ (8).

$$v_{p,m,b} = f_{p,m,b}\, v_{p,m,b\,\mathrm{bat}} - R_{\mathrm{DS_{on}}}\, i_{p,m,b} \tag{7}$$

$$i_{p,m,b\,\mathrm{bat}} = f_{p,m,b}\, i_{p,m,b} + i_{p,m,b\,\mathrm{sw}} \tag{8}$$

Switching losses for Si MOSFETs are challenging to model due to limited manufacturer data and the complexity

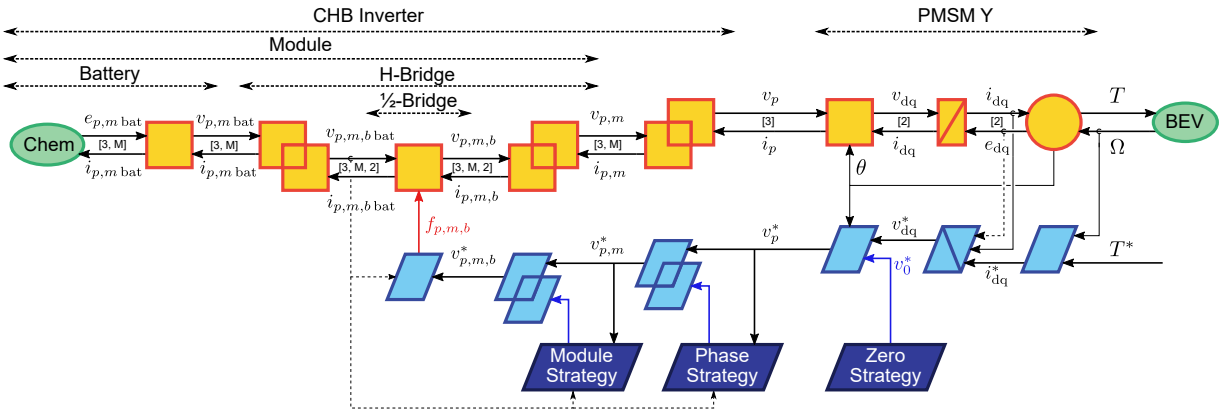

FIGURE 3. **Energetic Macroscopic Representation of a CHB Inverter with a Y-PMSM**

of analytical models [31]. This study employs simplified formulas (9), based on an Infineon application note, to calculate three key energy terms [13], [32] : channel conduction E_{mos}, diode recovery E_{rec}, and free-wheel diode conduction E_{fw}.

$$\begin{cases} E_{\text{mos}} = v_{p,m,b\,\text{bat}}\, i_{p,m,b}\, t_{\text{sw}}/2 \\ E_{\text{rec}} = Q_{\text{rr}}\, v_{p,m,b\,\text{bat}} \\ E_{\text{fw}} = (V_{\text{F}} + R_{\text{D}}\, i_{p,m,b})\; i_{p,m,b}\, t_{\text{fw}} \end{cases} \tag{9}$$

The energies calculated as described are utilized as an additional input current pulse on the battery side, as shown in (10), during a simulation period T_{sim} and when switching is detected, denoted as $\delta_{sw} = 1$.

$$i_{p,m,b\,\text{sw}} = \frac{E_{\text{mos}} + E_{\text{rec}} + E_{\text{fw}}}{T_{\text{sim}}\, v_{p,m,b\,\text{bat}}} \delta_{\text{sw}} \tag{10}$$

E. PERMANENT MAGNET SYNCHRONOUS MACHINE

The considered PMSM with salient poles is modeled in the Park domain, as described by (11) to (15). Its dynamics are governed by the inductances L_{d} and L_{q}, and the machine in Fig. 3 includes three key components: Park transform, inductive energy storage, and magneto-mechanical conversion.

$$\begin{cases} L_{\text{d}}(i_{\text{d}}, i_{\text{q}})\, i_{\text{d}} = \int (v_{\text{d}} - e_{\text{d}} - R_{\text{Cu}}(\omega)\, i_{\text{d}})\, \text{d}t \\ L_{\text{q}}(i_{\text{d}}, i_{\text{q}})\, i_{\text{q}} = \int (v_{\text{q}} - e_{\text{q}} - R_{\text{Cu}}(\omega)\, i_{\text{q}})\, \text{d}t \end{cases} \tag{11}$$

Copper losses are modeled by a series resistance $R_{\text{Cu}}(\omega)$, which depends on the speed ω and reflects the skin effect in conductors due to frequency. The inductance equation (11) are represented as an energy storage element in Figs. 3 and 8.

$$\begin{cases} e_{\text{d}} = -\omega\, \Phi_{\text{q}}(i_{\text{d}}, i_{\text{q}}) \\ e_{\text{q}} = +\omega\, \Phi_{\text{d}}(i_{\text{d}}, i_{\text{q}}) \end{cases} \tag{12}$$

Magnetic fluxes Φ_{d} and Φ_{q} are functions of currents i_{d} and i_{q}. These flows are used in the expressions for electromotive forces (emf) e_{d} and e_{q}, (12), as well as the electromagnetic torque T_{em}, (13). These equations takes place on Fig. 3 into the multi-physical conversion element.

$$T_{\text{em}} = n_{\text{p}}\, (\Phi_{\text{d}}(i_{\text{d}}, i_{\text{q}})\, i_{\text{q}} - \Phi_{\text{q}}(i_{\text{d}}, i_{\text{q}})\, i_{\text{d}}) \tag{13}$$

$$\omega = n_{\text{p}} \Omega \tag{14}$$

Iron losses are considered through a resistive torque T_{Fe} calculated for a torque-speed operating point, as shown in Equation 15. This element is highly dependent on the control law employed, so they must be determined together.

$$T = T_{\text{em}} - T_{\text{Fe}}(\Omega, T_{\text{em}}) \tag{15}$$

F. CONTROL AND ENERGY MANAGEMENT

The control of the system given by blue elements in Fig. 3 is succinctly presented below. More information are given in [26]. The system operates in torque control mode, with the BEV source effectively acting as an infinite inertia that dictates the machine's rotational speed. The magneto-mechanical element is inverted using predetermined machine maps aimed at minimizing current amplitude, referred to as Maximum Torque per Ampere (MTPA), which generate reference currents i_{d}^* and i_{q}^* based on reference torque T^* and measured speed Ω [33], [34]. The machine inductances inversion requires a current controller, implemented with a Proportional-Integral (PI) controller to generate target dq voltages. Prior to performing the inverse Park transform, a zero strategy may be introduced to modulate the neutral point potential.

After finalizing machine control, the CHB inverter must provide the requisite phase voltages v_p^*. Transitioning from 3 pieces of information to $3M$, the inversion of series module coupling, (1) and (2), allows for enhanced degrees of freedom. These are used to balanced the SoC among the various battery modules [26]. Additionally, as described in (3), each H-bridge has four available configurations for only three output states. The selection between the two zero-voltage configurations is governed by the Module Strategy block, which alternates between them. Finally, NLC is operated to recreate the sinusoids and determine the $6M$ command orders $f_{p,m,b}$.

As EMR is a flexible organisation tool, offering a quick and simple means to modify the configuration of complex systems by highlighting the coupling between different subsystems. This approach facilitates adjustments to the number of modules M and the quantity of battery cells per module N. Employing multiple strategy blocks within the proposed framework simplifies the implementation of various control strategies, such as alternative balancing methods or different modulation techniques. Ultimately, adopting the approach outlined in this paper enables the consideration of diverse losses and constraints for each subsystem. Consequently, it becomes feasible to separately quantify the contribution of each subsystem, as demonstrated in this study.

III. SIMULATION AND VALIDATION

A. SIMULATION OF OPERATING POINTS

The simulation is conducted based on the previously expressed models to analyze the waveforms and energetic quantities at each operating point (OP). Fig. 4 illustrates two critical OPs: high speed and high torque, both representing the same mechanical power of 30 kW.

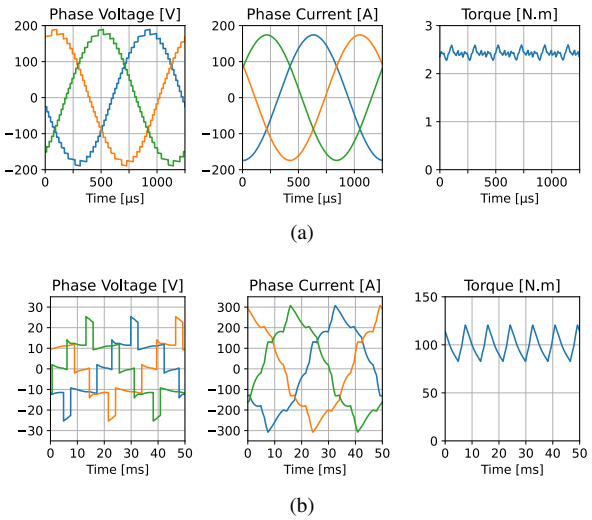

FIGURE 4. Scopes of critical operating points. (a) High speed and low torque (12 000 rpm, 2.5 N m). (b) High torque and low speed (300 rpm, 100 N m)

Impact of NLC is readily observed on these figures : voltages progress in steps resembling stairs to form the desired sinusoidal waveform. The current produced by the structure at Fig. 4a closely resembles a perfect sinusoid. Conversely, when lower voltage levels are utilized, as shown in Fig. 4b, fewer modules are activated, resulting in a degradation of the current waveform quality in the machine and consequently leading to torque ripple. Furthermore, high currents affect the voltage waveform, causing fluctuations in the voltage steps induced by phase currents.

B. EXPERIMENTAL VALIDATION

A real size static prototype have been developed with a battery capacity of 30 kWh [15] and a total of 72 modules, Fig. 5. Fig. 6 illustrates a real operating point of the CHB inverter connected to a driving machine. The voltage waveform exhibits distinct steps, indicating a poor low-frequency harmonic content. However, the current remains smooth, with only minor variations between pole pairs due to mechanical imperfections in the machine.

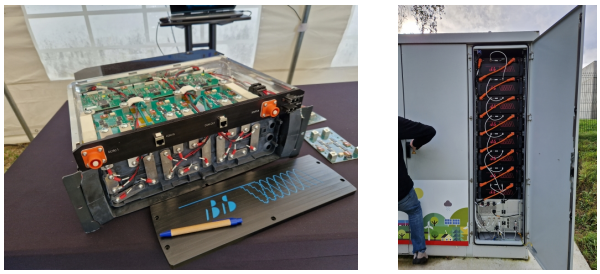

FIGURE 5. Photos of a 49-level CHB prototype [15]. (a) Cluster of 3 modules. (b) Phase rack.

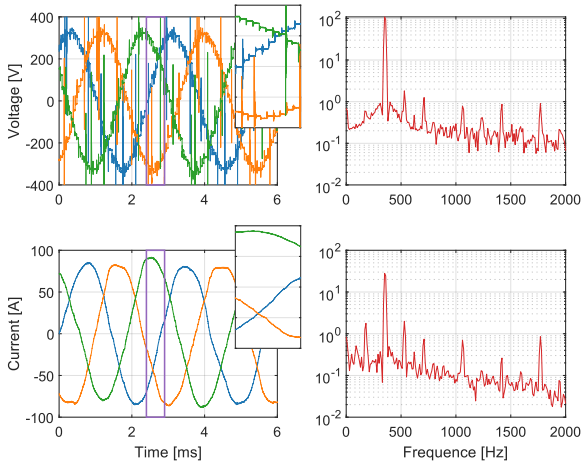

FIGURE 6. Experimental waveform at 5200 rpm and 40 N m

The voltage waveform contains many high-frequency spikes, the origin of which is difficult to determine. Electromagnetic interference is suspected to perturb the high-voltage differential probes through common-mode currents. The current waveform shows no spikes, which eliminates the hypothesis of high-frequency power transfer.

The primary objective of this article is to examine efficiency and consumption. Therefore, the validation of the simulated model will focus on energetic quantities. To achieve this, the efficiency of the CHB inverter (comprising power electronics and battery) is evaluated for three operating points through both experimental tests and simulations, as shown in Table 1.

The measurement tests are conducted during a discharge and recharge cycle of the battery. Initially, the State of Charge (SoC) is set to 90 %, and the battery is discharged to a SoC of 30 % using the driving machine at the selected

operating point. The energy flowing from the structure to the machine is measured using an integrator power meter HIOKI PW3337 with a 100 kHz bandwidth. Subsequently, the battery is charged using AC recharge mode with a known efficiency until reaching 90 % SoC again. The operating point efficiency is then deduced by considering the discharge and recharge energies, along with the recharge efficiency. A wide range of SoC variation enhances the precision of SoC estimation at start and end points but directly impacts efficiency due to the OCV variation, resulting in a mean value.

However, the duration of the tests directly depends on the power of the operating point and the battery capacity. The tests conducted in this study required up to 6 hours for each, and lower power tests would necessitate even more time, potentially spanning days. Therefore, the validation is limited to three medium-power points.

TABLE 1. Validation of efficiency estimation

Speed [rpm]	2000	3500	5200
Torque [N.m]	60	50	40
Experiment [%]	90.7	95.4	96.1
Simulation [%]	92.6	94.9	96.2

Table 1 demonstrates promising findings, with experimental results closely matching simulations, differing by less than two percentage points, thus validating the previous models.

IV. COMPARISON WITH TWO-LEVEL INVERTERS (2LI)

A. THREE STRUCTURES TO COMPARE

A two-level inverter (2LI) connects a high-voltage DC bus to a 3-phase traction machine using high-power switches like IGBTs or SiC MOSFETs. For a 400-volt DC bus, created by two parallel branches of 108 serial Li-ion NMC cells, the output line voltage is limited to 245 V due to the sinusoidal waveform. Higher DC bus voltages, such as 800 V with SiC MOSFETs, increase the available output voltage, as detailed in Table 2.

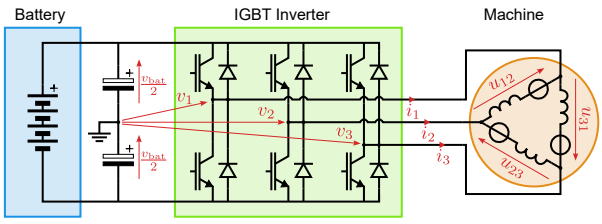

FIGURE 7. Two-level inverter connected to a Δ-configured machine

In the following, the SiC 2LI is used with a 800-volts DC bus at a switching frequency of 20 kHz, double of the IGBT 2LI in both cases [35]. To ensure a fair comparison of the impact on power electronics and the battery, the same machine is utilized in both cases. For consistency, the machine is configured as Δ for the IGBT setup and as Y for the SiC configuration. This configuration ensures that the available voltages observed by the machine are similar.

TABLE 2. Available voltage and PMSM configuration

	2L Inverter		CHB Inverter
Battery pack	108S2P	216S1P	24M4N
DC bus	400 V	800 V	-
Phase voltage	$\sqrt{2}/4\ SV_{\text{cell}}$		$\sqrt{2}/2\ MNV_{\text{cell}}$
	140 V	**280 V**	**250 V**
Line voltage	**245 V**	490 V	430 V
PMSM config.	Δ	Y	Y

The CHB configuration embed an increased number of cells compared to 2LI configurations, due to the AC grid connection constraint outlined in section II-B. This adjustment results in the phase and line voltages presented in Table 2. To ensure a fair comparison, the CHB will be Y-configured similar to the SiC MOSFET 2LI, while the IGBT 2LI will be Δ-configured.

The model of a two-level inverter (2LI) has been extensively studied, notably through the use of Energetic Macroscopic Representation (EMR) [28]. Fig. 8 shows the representation considered here.

Battery is modeled using a simple serial resistor approach to estimate battery losses. Dynamic behaviors are negligible in efficiency assessments and the battery's resistance and voltage are determined by the configuration and characteristics of its individual cells. Concerning power switches, conduction losses are considered with a voltage drop, depending on the transistor behavior. Switching losses are determined using energies provided by manufacturers and integrated as additional input current. Considering switching frequency is significantly higher than the desired signal frequency, duty cycles replace switching signals. Thus, simulation steps can be wider than switching period.

TABLE 3. Transistors references

Transistor	Reference	Producer	Volt. rat.
IGBT	FS400R07A1E3	Infineon	650 V
MOSFET Si	confidential	-	< 80 V
MOSFET SiC	ADP280120W3	STMicro	1200 V

B. EFFICIENCY IN TORQUE-SPEED FIELD

Simulations of the efficiency across a wide range of OPs are depicted in Fig. 9, illustrating efficiency maps in the Torque-Speed field for various structures: IGBT 2LI, SiC 2LI, and CHB. These maps consider efficiency across batteries, power electronics, and the machine.

Fig. 9 illustrates that the highest efficiency is attained with SiC MOSFET 2LI, reaching 95.3 %. IGBT 2LI shows a slower efficiency growth at low speeds, whereas SiC 2LI exhibit some enhancements.CHB proposes significant improvements in this aspect with efficiency higher than

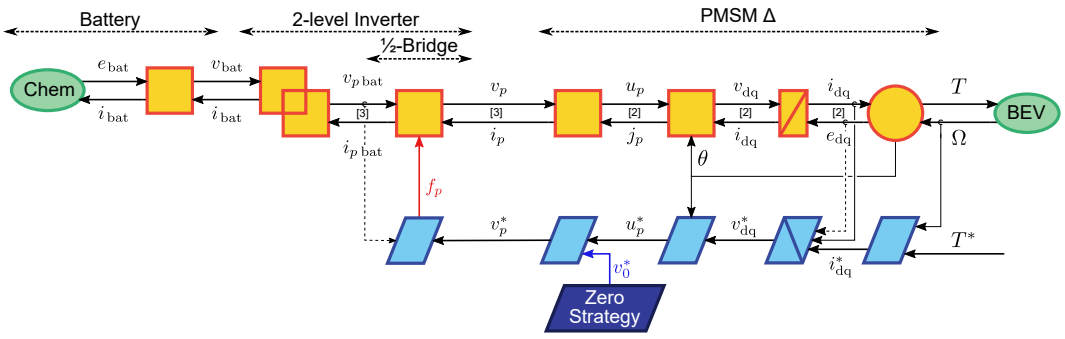

FIGURE 8. Energetic Macroscopic Representation of a 2L-Inverter with a △-PMSM

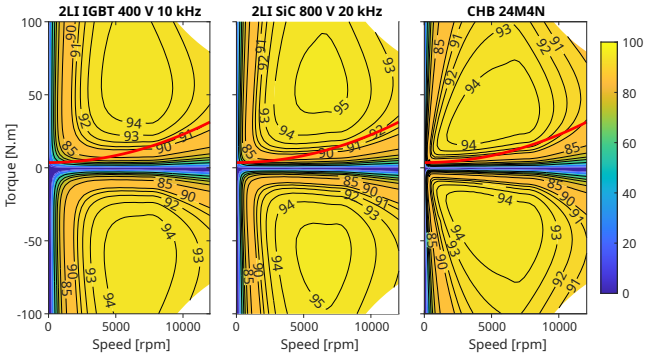

FIGURE 9. Efficiency maps of the IGBT and SiC 2LI, and CHB powertrains. The red curve represents the constant speed torque of the vehicle.

90 % since speed exceed 400 rpm, while speed needs to be increased to 1200 rpm for SiC to achieve the same result. Hence, an enhancement in vehicle efficiency during urban cycles can be expected.

Regenerative braking stands as one of the most significant improvements in electric vehicles compared to internal combustion engine counterparts. Nevertheless, its indiscriminate use can lead to inefficiencies, with certain areas of the Torque-Speed field resulting in zero efficiency at low speed, wherein battery energy is consumed for braking purposes. Hence, the implementation of braking strategies becomes imperative in vehicles [36]. As illustrated in Fig. 9, these inefficient regions are considerably smaller for SiC 2LI compared to IGBT 2LI, and even smaller for CHB configurations.

Finally, vehicles are predominantly operated at low power levels, which plays to the advantage of CHB configurations since their higher-efficiency regions typically align with lower power outputs compared to 2LI setups.

V. ELECTRIC VEHICLE AND REALISTIC CONDITIONS

A. METHODOLOGY

Simulating a driving cycle (20 minutes) with a simulation step compatible with electric period representation (8 ms at 100 km/h) can be computationally expensive. While estimating the energetic behavior of a PWM-driven system is sufficient with an average model [13], [28], the Nearest Level Control strategy involves few switchings, sometimes using only a few voltage levels. Therefore, simulations should deliver accurate waveforms to ensure precise estimations of switching losses.

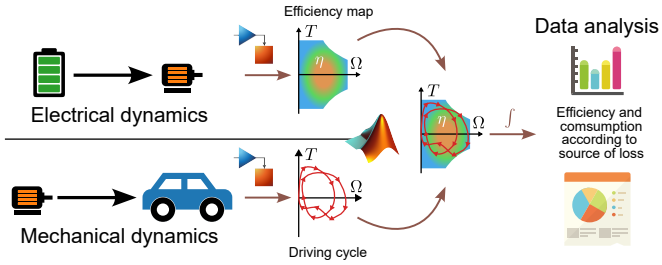

FIGURE 10. Methodology, separated electrical and mechanical simulation

To avoid costly computation times, simulations are divided between electrical and mechanical ones, which is possible because mechanical dynamics are significantly slower than electrical ones. This process is illustrated in Fig. 10: a first simulation campaign is conducted from the battery to the machine to obtain efficiency maps in the torque-speed field, followed by a second campaign from the machine output to the road to generate driving cycle trajectories in the same field. The resulting data are then merged to determine the efficiency and consumption of each element in the traction chain for driving cycles. This approach gives similar results as an unique simulation while reducing the computational burdens.

A simplified longitudinal model of the BEV is employed, assuming straight motion without considering curves. Consequently, the torques of both sides wheels are assumed to be perfectly equal. These hypotheses result in the EMR depicted in Fig. 11. Three energy sources are represented: the electric drive (ED), the mechanical brake, and the environment.

This model is a classic example of EMR vehicle representation. The equations and the EMR are detailed in [37], [38], considering three dissipative terms: gearbox efficiency, drag coefficient, and rolling resistance. Important parameters are summarized in Table 4.

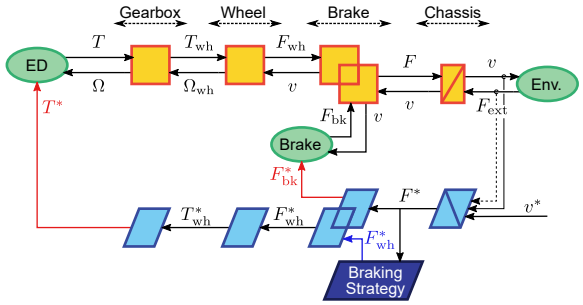

FIGURE 11. EMR of an electric vehicle

TABLE 4. Vehicle parameters

	Symbol	Value
Vehicle mass	m_{ev}	1600 kg
Dynamic mass	m_{dyn}	1635 kg
Gearbox ratio	r_{gb}	9.8
Wheel radius	R_{wh}	350 mm
Drag coefficient	SC_{x}	0.645 m^2
Rolling resistance	C_{rr}	6.2×10^{-3}
Air density	ρ	1.2 $\mathrm{kg/m}^3$

B. CONSTANT SPEED STUDY

Given the vehicle model, the torque required to sustain a constant speed is computed (16), and depicted in red on Fig. 9. The efficiency corresponding to this red curve is determined on Fig. 12. Moreover, the consumption C attributable to the traction chain can be evaluated as the ratio of expended energy per travelled distance (driving cycle) or the ratio of expended power divided by the vehicle speed v.

$$T = \frac{R_{\mathrm{wh}}}{\eta_{\mathrm{gb}}\, r}\left(C_{\mathrm{rr}} mg + \frac{1}{2}\rho S C_{\mathrm{x}}\left(\frac{R_{\mathrm{wh}}}{r}\Omega\right)^2\right) \tag{16}$$

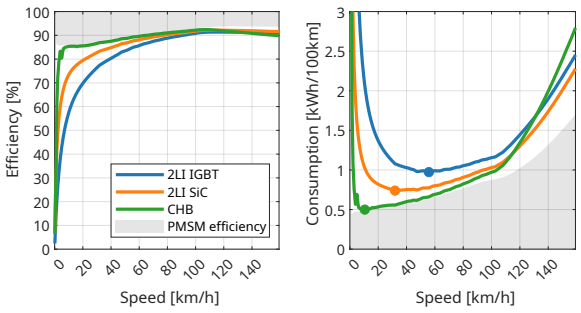

FIGURE 12. Efficiency and consumption at constant speed, limited to the traction chain

Fig. 12 illustrates superior efficiency and lower consumption for CHB in comparison to SiC and IGBT 2LI at low speeds. While SiC demonstrates better performance than IGBT in this setup, CHB nearly reaches the minimum achievable consumption owing to the machine's performance constraints and despite using Nearest Level Control. The lowest consumption for each structure varies with speed and is less (both in speed and consumption) for CHB compared to SiC and IGBT, as outlined in Table 5.

TABLE 5. Lowest constant speed consumption from battery to machine

	CHB	2LI SiC	2LI IGBT
Speed [km/h]	10.5	31.9	55.8
Consumption [kWh/100km]	0.50	0.74	0.97

On the contrary, CHB exhibits the highest consumption at high speeds exceeding 130 km/h, performing worse than IGBT. Nonetheless, this observation needs to be contextualized within the influence of mechanical transmission and aerodynamic forces, which predominantly affect consumption at high speeds. Beyond 40 km/h, the powertrain contributes to less than 20% of the vehicle's consumption, a proportion that diminishes towards 10% at higher speeds.

By nature, the constant speed approach neglects vehicle dynamics and only examines a limited portion of the torque-speed field. However, in reality, a significant portion of a vehicle's energy consumption occurs during dynamic phases. Thus, driving cycles are essential for a more comprehensive evaluation.

C. DRIVING CYCLE ANALYSIS

To evaluate and compare vehicule's consumptions in realistic conditions, several driving cycles have been developped: WLTC, USA City, Artemis... Here, INRETS cycles will be used as they are representative of diverse European driving scenarios, encompassing slow urban traffic (UL1), smooth urban traffic (UF1), road (R1), highway (A1) conditions [27].

Fig. 13 illustrates the exploration of the torque-speed field by each of speed profile. As expected, urban driving cycles predominantly operate at low speeds, while road and highway profiles venture into higher speeds. Additionally, road and highway cycles exhibit greater torque utilization for more significant accelerations. Notably, the A1 cycle mainly operates at high speeds and low torque, indicating constant high-speed driving.

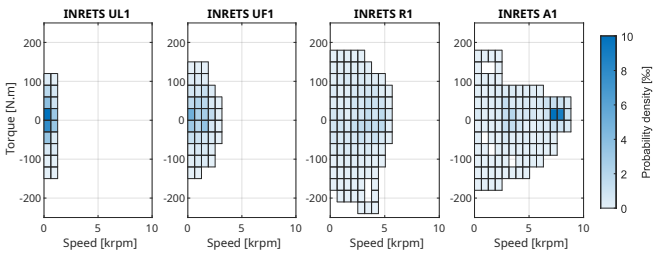

FIGURE 13. Torque-Speed histogram of four driving cycles

The vehicle's comsumption can be split into four terms: three for the powertrain (battery, power electronics and machine) and one for the rest (mechanical transmission, rolling and aerodynamic resistance) grouped under "rolling" term. The machine and rolling consumptions are independent of the converter structure and remain consistent across different structures for the same driving cycle.

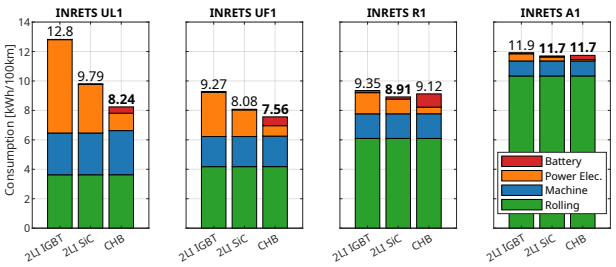

FIGURE 14. Consumption of the EV for four driving cycles

Fig. 14 shows the simulated consumption of each element for the considered cycles. The use of CHB inverter allows a great reduction of the consumption in slow urban speed profile (UL1) compared to IGBT and SiC. CHB losses are no longer located in power electronics but also in batteries. High speed driving cycle illustrates the little impact of power electronics and battery on the consumption. In this configuration, no significant gains are expected from replacing the 2LI architecture.

VI. DISCUSSION

The modeling of the traction chain from the battery to the road is clearly stated in this paper, using EMR and forward methodology for clarity and accuracy. Literacy traditionally considers less energetic element and without interaction between them. It is based on existing models that simplify reality to limit computational power and time required to simulate the entire system and its energetic performances. For instance, only a static model of the batteries is considered. In reality, the slowest time constant (around 10 seconds) can have different consequences due to the specific stress of a CHB using NLC. The error has been evaluated for a classic structure and is negligible in this case [39], but not yet for the cascaded structure. Accounting for this would require significantly heavier calculations, as well as the consideration of a parallel capacitor to absorb high frequencies, as is done in real-world applications.

The machine model used here does not consider the effect of harmonics on losses, particularly iron losses [40]. The spectrum produced by the CHB is significantly different from that of a conventional inverter, which has implications for the machine's performance. Future studies will need to assess the impact on efficiency and mechanical stress.

The integration of MOSFET transistor switching losses is based on simplified models validated through simulation [13]. Although current circuit simulations provide results accurately, these models still involve significant simplifications. However, because the use of NLC reduces the number of switching events, switching losses constitute a minor fraction of total losses, making the resulting error negligible.

Experimental validation was successfully conducted within a specific range of the torque-speed plane, despite certain mechanical and electrical constraints inherent to the experimental setup. Furthermore, the current measurement protocol necessitates longer test durations for lower power levels, it allowed the collection of valuable data points. Future improvements to the test bench would enable access to a broader torque-speed range, and complementary optimizations, such as reducing battery capacity, are expected to further accelerate the testing process, thereby increasing the volume of data collected for deeper analysis.

Nonetheless, the individual models have been validated in the literature, and the results obtained are consistent with the comparison approach used subsequently. This paper effectively clarifies the models employed, facilitating future improvements to refine the reported results. The key contribution of this work lies in the methodology used to model and compare different structures.

The comparative results obtained prompt further investigation. Specifically, the change in stress as the current move from DC to AC, and increased battery losses, raise questions about battery aging. The literature remains sparse on this topic, despite some recent studies [25].

Finally, an important finding of the study is that improvements in consumption are achieved primarily at low-speed operating points which are highly important as many EVs are used only in urban area. The CHB then extends the limits of the 2LI, and the limiting factor becomes the machine itself. Conversely, at high speeds, the traction chain has minimal impact on consumption, reducing the benefit of improving efficiency in these conditions.

VII. CONCLUSION

A novel powertrain based on a CHB inverter with 24 modules per phase is proposed to enhance the scalability, the efficiency and the driving range of EVs. Combining these benefits with the structure's advantages in terms of modularity, repairability, resilience, and versatility may make this powertrain a key asset for future EVs.

To demonstrate the interest of this electric drive in terms of efficiency, this article has developed a new methodology to consider the switching losses of the Cascaded H-Bridge (CHB) inverter driving by nearest level control (NLC). As this type of inverter control causes significant variations in switching frequency over time, the evaluation of the losses is complex and waste a huge amount of time. To reduce the computation time, the electric dynamic is performed first to calculate the losses of the different components of the powertrain and then include them to a global vehicle simulation tool.

By using the tool developed, a comprehensive analysis of component-level losses and system-level energy consumption is performed. As many papers on multilevel converters in the literature performed a comparison with a low number of operating points, our tool allows us to study any operating condition and in particular enables the evaluation of driving cycles which are classically performed in electric vehicle studies.

A comparative study of power converters structure for EV based on SiC MOSFET 2LI, IGBT 2LI, and CHB inverters shown that the CHB inverter achieves comparable or superior performance to other structures. An analysis of efficiency maps, constant-speed curves, and driving cycles reveals that the CHB especially exhibits superior efficiency and lower consumption at low speeds compared to SiC and IGBT 2LI. However, at very high speeds, CHB shows higher consumption than SiC 2LI, although this is mitigated by the dominant influence of mechanical transmissions and aerodynamic forces at these speeds. Implementing a CHB inverter causes a significant reduction in consumption during urban cycles compared to IGBT and SiC options. Nonetheless, a limitation remains in maintaining the same vehicle mass across all configurations.

Despite CHB-based EV offering improved efficiencies, our findings suggest an increase in battery losses. This, combined with changes in current loads, could potentially affect the lifespan of battery cells. Further investigation is required.

The CHB-based EV model and its control, presented in this paper, establish a versatile simulation tool that integrates all constraints and strategies of the real system, including losses. This tool has been validated through comparison with the real system. Moreover, this method facilitates the adjustment of system parameters and the implementation of various control strategies. From this tool, it is possible to simulate a wide range of battery modules, especially for high module numbers such as 24 in this article. Moving forward, future studies will focus on optimizing the distribution of cells within the structure to determine the optimal division (M, N) of the battery into modules. Altering the cell distribution affects the waveform, and its implications on machine performance, as well as harmonic content during recharge, will need to be evaluated.

The control strategy used here (NLC) has the advantage of requiring very few switching. Contrary to initial expectations in the literature regarding its performance at low speeds, our findings suggest that NLC can be an efficient choice when a sufficient number of levels are available. Exploring alternative strategies like pulse width modulation may improve waveform quality. A comparative study on the impact of these strategies on efficiency, cell and machine aging, and harmonic distortion could provide valuable insights.

APPENDIX

TABLE 6. Nomenclature

	Symbol	Unit
Bridge index	b	-
Rolling resistance	C_{rr}	-
Battery open circuit voltage	e_{bat}	V
PMSM Park electromotive forces	$e_{\mathrm{d}},\ e_{\mathrm{q}}$	V
Channel conduction energy	E_{mos}	J
Diode recovery energy	E_{rec}	J
Diode conduction energy	E_{fw}	J
Switching energy	E_{sw}	J
Switching command (2LI)	f_p	-
Switching command (CHB)	$f_{p,m,b}$	-
Vehicle force	F	N
External force	F_{ext}	N
Braking force	F_{bk}	N
Wheel force	F_{wh}	N
PMSM Park currents	$i_{\mathrm{d}},\ i_{\mathrm{q}}$	A
PMSM Park current references	$i_{\mathrm{d}}^{*},\ i_{\mathrm{q}}^{*}$	A
Battery current	i_{bat}	A
Phase current	i_p	A
Phase battery current (2LI)	$i_{p\,\mathrm{bat}}$	A
Module output current	$i_{p,m}$	A
Module battery current	$i_{p,m\,\mathrm{bat}}$	A
Half-bridge output current	$i_{p,m,b}$	A
Half-bridge battery current	$i_{p,m,b\,\mathrm{bat}}$	A
Switching additional current (CHB)	$i_{p,m,b\,\mathrm{sw}}$	A
PMSM Park inductances	$L_{\mathrm{d}},\ L_{\mathrm{q}}$	H
Module index	m	-
Vehicle mass	m_{ev}	kg
Dynamic mass	m_{dyn}	kg
Number of modules (CHB)	M	-
Number of pole pairs	n_p	-
Number of cells (CHB)	N	-
Phase index	p	-
Number of parallel battery cells (2LI)	P	-
Recovery charge	Q_{rr}	C
Gearbox ratio	r_{gb}	-
Diode conduction resistance (CHB)	R_{D}	Ω
MOSFET conduction resistance	$R_{\mathrm{DS_{on}}}$	Ω
PMSM conduction resistance	R_{Cu}	Ω
Wheel radius	R_{wh}	m
Number of serial battery cells (2LI)	S	-
Drag coefficient	SC_{x}	m^2
Switching duration	t_{sw}	s
Free-wheel duration	t_{fw}	s
PMSM Mechanical torque	T	N m
PMSM Mechanical torque reference	T^{*}	N m
Electromagnetic torque	T_{em}	N m
Iron losses torque	T_{Fe}	N m
Wheel torque	T_{wh}	N m
Simulation period	T_{sim}	s
Vehicle speed	v	$\mathrm{m\,s^{-1}}$

TABLE 6. Nomenclature (continued)

	Symbol	Unit
Battery voltage	v_{bat}	V
PMSM Park voltages	$v_{\mathrm{d}},\ v_{\mathrm{q}}$	V
PMSM Park voltage references	$v_{\mathrm{d}}^*,\ v_{\mathrm{q}}^*,\ v_0^*$	V
Phase voltage	v_p	V
Phase voltage reference	v_p^*	V
Module output voltage	$v_{p,m}$	V
Module output voltage reference	$v_{p,m}^*$	V
Module battery voltage	$v_{p,m\,\mathrm{bat}}$	V
Half-bridge output voltage	$v_{p,m,b}$	V
Half-bridge output voltage reference	$v_{p,m,b}^*$	V
Half-bridge battery voltage	$v_{p,m,b\,\mathrm{bat}}$	V
Diode forward voltage (CHB)	V_{F}	V
Switching indicator	δ_{sw}	-
Gearbox effiency	η_{gb}	-
Air density	ρ	kg/m^3
PMSM Park magnetic fluxes	$\Phi_{\mathrm{d}},\ \Phi_{\mathrm{q}}$	Wb
Electrical speed	ω	rad s^{-1}
Mechanical speed	Ω	rad s^{-1}
Wheel speed	Ω_{wh}	rad s^{-1}

ACKNOWLEDGEMENT

This document results of the IBIS research project funded by ADEME under the French Government's "Programme d'investissements d'avenir (PIA)."

References

[1] K. Calvin, D. Dasgupta, G. Krinner, *et al.*, "IPCC, 2023: Climate Change 2023: Synthesis Report. Contribution of Working Groups I, II and III to the Sixth Assessment Report of the Intergovernmental Panel on Climate Change [Core Writing Team, H. Lee and J. Romero (eds.)]," Intergovernmental Panel on Climate Change (IPCC), Geneva, Switzerland, Tech. Rep., Jul. 2023, pp. 1–34. DOI: 10.59327/IPCC/AR6-9789291691647. (visited on 02/12/2024).

[2] L. Paoli, A. Dasgupta, and S. McBain, "Electric Vehicles," IEA, Paris, Tech. Rep., 2022. (visited on 02/06/2023).

[3] IEA, *Global EV Outlook 2023 : Trends in electric light-duty vehicles*, https://www.iea.org/energy-system/transport/electric-vehicles, Apr. 2023. (visited on 01/08/2024).

[4] M. Jafari, A. Gauchia, S. Zhao, K. Zhang, and L. Gauchia, "Electric Vehicle Battery Cycle Aging Evaluation in Real-World Daily Driving and Vehicle-to-Grid Services," *IEEE Transactions on Transportation Electrification*, vol. 4, no. 1, pp. 122–134, Mar. 2018, ISSN: 2332-7782. DOI: 10.1109/TTE.2017.2764320. (visited on 02/21/2024).

[5] A. Ndiaye, R. German, A. Bouscayrol, *et al.*, "Impact of the User Charging Practice on the Battery Aging in an Electric Vehicle," *IEEE Transactions on Vehicular Technology*, pp. 1–10, 2024, ISSN: 1939-9359. DOI: 10.1109/TVT.2024.3356116. (visited on 01/30/2024).

[6] X. Lai, Q. Chen, X. Tang, *et al.*, "Critical review of life cycle assessment of lithium-ion batteries for electric vehicles: A lifespan perspective," *eTransportation*, vol. 12, p. 100 169, May 2022, ISSN: 2590-1168. DOI: 10 . 1016 / j . etran . 2022 . 100169. (visited on 02/09/2024).

[7] N. Wassiliadis, M. Steinsträter, M. Schreiber, *et al.*, "Quantifying the state of the art of electric powertrains in battery electric vehicles: Range, efficiency, and lifetime from component to system level of the Volkswagen ID.3," *eTransportation*, vol. 12, p. 100 167, May 2022, ISSN: 2590-1168. DOI: 10.1016/j.etran.2022.100167. (visited on 02/09/2024).

[8] D.-D. Tran, M. Vafaeipour, M. El Baghdadi, *et al.*, "Thorough state-of-the-art analysis of electric and hybrid vehicle powertrains: Topologies and integrated energy management strategies," *Renewable and Sustainable Energy Reviews*, vol. 119, p. 109 596, Mar. 2020, ISSN: 1364-0321. DOI: 10.1016/j.rser.2019.109596. (visited on 02/15/2024).

[9] L. Komsiyska, T. Buchberger, S. Diehl, *et al.*, "Critical Review of Intelligent Battery Systems: Challenges, Implementation, and Potential for Electric Vehicles," *Energies*, vol. 14, no. 18, p. 5989, Jan. 2021, ISSN: 1996-1073. DOI: 10.3390/en14185989. (visited on 02/07/2022).

[10] Z. Zhao, H. Hu, Z. He, *et al.*, "Power Electronics-Based Safety Enhancement Technologies for Lithium-Ion Batteries: An Overview From Battery Management Perspective," *IEEE Transactions on Power Electronics*, vol. 38, no. 7, pp. 8922–8955, Jul. 2023, ISSN: 1941-0107. DOI: 10 . 1109 / TPEL . 2023 . 3265278. (visited on 02/09/2024).

[11] M. Quraan, T. Yeo, and P. Tricoli, "Design and Control of Modular Multilevel Converters for Battery Electric Vehicles," *IEEE Transactions on Power Electronics*, vol. 31, no. 1, pp. 507–517, Jan. 2016, ISSN: 1941-0107. DOI: 10.1109/TPEL.2015.2408435.

[12] L. Tolbert, F. Z. Peng, and T. Habetler, "Multilevel converters for large electric drives," *IEEE Transactions on Industry Applications*, vol. 35, no. 1, pp. 36–44, Jan. 1999, ISSN: 1939-9367. DOI: 10.1109/28.740843.

[13] F. Chang, O. Ilina, M. Lienkamp, and L. Voss, "Improving the Overall Efficiency of Automotive Inverters Using a Multilevel Converter Composed of Low Voltage Si mosfets," *IEEE Transactions on Power Electronics*, vol. 34, no. 4, pp. 3586–3602, Apr. 2019, ISSN: 1941-0107. DOI: 10.1109/TPEL.2018.2854756.

[14] L. Mathe, P. Dan Burlacu, E. Schaltz, and R. Teodorescu, "Battery pack state of charge balancing algorithm for cascaded H-Bridge multilevel converters," in *2016 IEEE 16th International Conference on Environment and Electrical Engineering (EEEIC)*, Jun. 2016, pp. 1–6. DOI: 10.1109/EEEIC.2016.7555737.

[15] J.-C. Lefebvre and V. Gillot, *IBIS: Stellantis and Saft Reveal a Smarter, More Efficient Battery for Autos and Stationary Power*, https://www.stellantis.com/en/news/press-releases/2023/july/ibis-stellantis-and-saft-reveal-a-smarter-more-efficient-battery-for-autos-and-stationary-power, Jul. 2023. (visited on 02/13/2024).

[16] R. J. Kuhudzai, *Distributed Battery Management Inverters: The New Frontier For Life-Extended, Cost-Reduced Batteries*, https://cleantechnica.com/2023/12/12/distributed-battery-management-inverters-the-new-frontier-for-life-extended-cost-reduced-batteries/, Dec. 2023. (visited on 10/02/2024).

[17] F. Eroğlu, M. Kurtoğlu, and A. M. Vural, "Bidirectional DC–DC converter based multilevel battery storage systems for electric vehicle and large-scale grid applications: A critical review considering different topologies, state-of-charge balancing and future trends," *IET*

Renewable Power Generation, vol. 15, no. 5, pp. 915–938, 2021, ISSN: 1752-1424. DOI: 10.1049/rpg2.12042. (visited on 02/09/2024).

[18] L. Maharjan, S. Inoue, H. Akagi, and J. Asakura, "State-of-Charge (SOC)-Balancing Control of a Battery Energy Storage System Based on a Cascade PWM Converter," *IEEE Transactions on Power Electronics*, vol. 24, no. 6, pp. 1628–1636, Jun. 2009, ISSN: 1941-0107. DOI: 10.1109/TPEL.2009.2014868.

[19] J. Fang, F. Blaabjerg, S. Liu, and S. M. Goetz, "A Review of Multilevel Converters With Parallel Connectivity," *IEEE Transactions on Power Electronics*, vol. 36, no. 11, pp. 12 468–12 489, Nov. 2021, ISSN: 1941-0107. DOI: 10.1109/TPEL.2021.3075211.

[20] T. Aldhanhani, A. Abraham, W. Hamidouche, and M. Shaaban, "Future Trends in Smart Green IoV: Vehicle-to-Everything in the Era of Electric Vehicles," *IEEE Open Journal of Vehicular Technology*, vol. 5, pp. 278–297, 2024, ISSN: 2644-1330. DOI: 10.1109/OJVT.2024.3358893. (visited on 10/02/2024).

[21] F. Eroglu, M. Kurtoglu, A. Eren, and A. M. Vural, "A novel adaptive state-of-charge balancing control scheme for cascaded H-bridge multilevel converter based battery storage systems," *ISA Transactions*, Oct. 2022, ISSN: 0019-0578. DOI: 10.1016/j.isatra.2022.09.044. (visited on 01/23/2023).

[22] M. Vasiladiotis and A. Rufer, "Balancing control actions for cascaded H-bridge converters with integrated battery energy storage," in *2013 15th European Conference on Power Electronics and Applications (EPE)*, Sep. 2013, pp. 1–10. DOI: 10.1109/EPE.2013.6634337. (visited on 02/09/2024).

[23] A. Ali and H. A. Khalid, "Comparative Analysis of Two-Level and Multilevel CHB Topologies for EV Drivetrain," in *2023 International Conference on Emerging Power Technologies (ICEPT)*, May 2023, pp. 1–6. DOI: 10.1109/ICEPT58859.2023.10152403.

[24] B. McGrath and D. Holmes, "Multicarrier PWM strategies for multilevel inverters," *IEEE Transactions on Industrial Electronics*, vol. 49, no. 4, pp. 858–867, Aug. 2002, ISSN: 1557-9948. DOI: 10.1109/TIE.2002.801073.

[25] O. Theliander, A. Kersten, M. Kuder, *et al.*, "Battery Modeling and Parameter Extraction for Drive Cycle Loss Evaluation of a Modular Battery System for Vehicles Based on a Cascaded H-Bridge Multilevel Inverter," *IEEE Transactions on Industry Applications*, vol. 56, no. 6, pp. 6968–6977, Nov. 2020, ISSN: 1939-9367. DOI: 10.1109/TIA.2020.3026662.

[26] C. Mayet, D. Labrousse, R. Bkekri, F. Roy, and G. Pongnot, "Energetic Macroscopic Representation and Inversion-Based Control of a Multi-Level Inverter with Integrated Battery for Electric Vehicles," in *2021 IEEE Vehicle Power and Propulsion Conference (VPPC)*, présentation orale par C. Mayet, Gijon, Spain: IEEE, Oct. 2021, pp. 1–6. DOI: 10.1109/VPPC53923.2021.9699228.

[27] M. André, "The ARTEMIS European driving cycles for measuring car pollutant emissions," *Science of The Total Environment*, Highway and Urban Pollution, vol. 334–335, pp. 73–84, Dec. 2004, ISSN: 0048-9697. DOI: 10.1016/j.scitotenv.2004.04.070. (visited on 01/26/2023).

[28] A. Desreveaux, E. Labouré, O. Bethoux, *et al.*, "Fast Computational Dynamic Model of Traction Drive for Electric Vehicles," in *2022 IEEE Vehicle Power and Propulsion Conference (VPPC)*, Nov. 2022, pp. 1–6. DOI: 10.1109/VPPC55846.2022.10003383.

[29] P. Arboleya, C. Mayet, B. Mohamed, J. A. Aguado, and S. de la Torre, "A review of railway feeding infrastructures: Mathematical models for planning and operation," *eTransportation*, vol. 5, p. 100 063, Aug. 2020, ISSN: 2590-1168. DOI: 10.1016/j.etran.2020.100063. (visited on 02/09/2024).

[30] A. Bouscayrol and B. Lemaire-Semail, "Energetic macroscopic representation and inversion-based control," in *Encyclopedia of Electrical and Electronic Power Engineering*, J. García, Ed., Oxford: Elsevier, Jan. 2023, pp. 365–375, ISBN: 978-0-12-823211-8. DOI: 10.1016/B978-0-12-821204-2.00117-3. (visited on 02/15/2023).

[31] D. Christen and J. Biela, "Analytical Switching Loss Modeling Based on Datasheet Parameters for mosfets in a Half-Bridge," *IEEE Transactions on Power Electronics*, vol. 34, no. 4, pp. 3700–3710, Apr. 2019, ISSN: 1941-0107. DOI: 10.1109/TPEL.2018.2851068.

[32] D. D. Graovac, M. Pürschel, and A. Kiep, *MOSFET Power Losses Calculation Using the Datasheet Parameters*, Jun. 2006.

[33] S. Morimoto, Y. Tong, Y. Takeda, and T. Hirasa, "Loss minimization control of permanent magnet synchronous motor drives," *IEEE Transactions on Industrial Electronics*, vol. 41, no. 5, pp. 511–517, Oct. 1994, ISSN: 1557-9948. DOI: 10.1109/41.315269.

[34] R. Ni, D. Xu, G. Wang, *et al.*, "Maximum Efficiency Per Ampere Control of Permanent-Magnet Synchronous Machines," *IEEE Transactions on Industrial Electronics*, vol. 62, no. 4, pp. 2135–2143, Apr. 2015, ISSN: 1557-9948. DOI: 10.1109/TIE.2014.2354238.

[35] I. Aghabali, J. Bauman, P. J. Kollmeyer, *et al.*, "800-V Electric Vehicle Powertrains: Review and Analysis of Benefits, Challenges, and Future Trends," *IEEE Transactions on Transportation Electrification*, vol. 7, no. 3, pp. 927–948, Sep. 2021, ISSN: 2332-7782. DOI: 10.1109/TTE.2020.3044938. (visited on 09/28/2023).

[36] F. Naseri, E. Farjah, and T. Ghanbari, "An Efficient Regenerative Braking System Based on Battery/Supercapacitor for Electric, Hybrid, and Plug-In Hybrid Electric Vehicles With BLDC Motor," *IEEE Transactions on Vehicular Technology*, vol. 66, no. 5, pp. 3724–3738, May 2017, ISSN: 1939-9359. DOI: 10.1109/TVT.2016.2611655.

[37] R. German, S. Shili, A. Desreveaux, *et al.*, "Dynamical Coupling of a Battery Electro-Thermal Model and the Traction Model of an EV for Driving Range Simulation," *IEEE Transactions on Vehicular Technology*, vol. 69, no. 1, pp. 328–337, Jan. 2020, ISSN: 0018-9545, 1939-9359. DOI: 10.1109/TVT.2019.2955856. (visited on 09/01/2023).

[38] G. Pongnot, C. Mayet, and D. Labrousse, "Comparison of Different Braking Strategies to Improve the Energy Recovery of an Electric Vehicle Based on Cascaded H-Bridge Inverter with Batteries," in *2023 IEEE Vehicle Power and Propulsion Conference (VPPC)*, présentation orale par C. Mayet, Milano, Italia, Oct. 2023, pp. 1–6. DOI: 10.1109/VPPC60535.2023.10403284. (visited on 02/27/2024).

[39] D. Ramsey, R. German, A. Bouscayrol, and L. Boulon, "Comparison of equivalent circuit battery models for energetic studies on electric vehicles," in *2020 IEEE Vehicle Power and Propulsion Conference (VPPC)*, Gijon, Spain, 2020. DOI: 10.1109/VPPC49601.2020.9330891. (visited on 09/17/2024).

[40] R. Jardot, G. Krebs, A. Lahlou, F. Roy, and C. Marchand, "Order Reduction of a Frequency Magneto-Dynamic Problem for the Calculation of Copper Losses," in *ICEM 2024*, Turin, Italy: Symposium, Aug. 2024. (visited on 09/17/2024).

Gaël Pongnot received the M.S. degree in Electrical engineering from École normale supérieure Paris-Saclay, Université Paris-Saclay, France, in 2021. He is currently working toward the Ph.D. degree at SATIE laboratory, Université Paris-Saclay, ENS Paris-Saclay, France. His research interests include power electronics converters, graphical description, modeling, simulation, and energy management for electric transportation.

Anatole Desreveaux received the MS degree on control and Electrical engineering in 2016 and the Ph.D. degree in electrical engineering in 2020, both from the University of Lille, France. From 2020 to 2021, He held a postdoctoral position within the PANDA H2020 European project at the University of Lille. From 2021 to 2023, he was a postdoc at Centrale-Supelec – Université Paris-Saclay in the GeePs and L2S laboratories. Since 2023, he is associate professor at the Conservatoire National des Arts et Métiers of Paris and at the SATIE laboratory. His research interests include graphical description, modeling, control, simulation, and energy management of Electrified Vehicles.

Clément Mayet (Member, IEEE) received the Ph.D. degree in electrical engineering from the University of Lille, France, in 2016. Then, he held a post-doctoral position at the University of Lille and the L2EP. From 2017 to 2018, he was a Senior Researcher with the MOBI Research Group, Vrije Universiteit of Brussels, Belgium. From 2018 to 2023, he was Associate Professor at the Conservatoire National des Arts et Métiers (CNAM) de Paris and member of the SATIE Laboratory. Since 2023, he is now Associate Professor at University of Lille and the L2EP, France. His research interests include graphical descriptions (Energetic Macroscopic Representation), modelling, control, energy management, and hardware-in-the-loop simulation of Electric and Hybrid Vehicles (EVs and HEVs).

Denis Labrousse was born in France, in 1981. He received the M.S. and Ph.D. degrees in electrical engineering from the Ecole Normale Supérieure de Cachan (ENS de Cachan), Cachan, France, in 2007 and 2010, respectively. His Ph.D. degree was focused on electromagnetic compatibility of power electronics converters and was performed with the team Integrated Power Electronics and Materials in the Laboratory of Systèmes et Applications des Technologies de l'Information et de l'Energie, ENS de Cachan, Cachan. Since September 2012, he has been an Assistant Professor at the Conservatoire National des Arts et Métiers, Paris, France, where he carries out research at the SATIE Laboratory. His principal fields of research include the EMC of the power electronics converters.